JOURNAL OF MATERIALS SCIENCE 19 (1984) 1957–1968

Investigation of the nature of micro-indentation hardness gradients below sliding contacts in five copper alloys worn against 52100 steel

PETER J. BLAU
Metallurgy Division, National Bureau of Standards, Washington, DC 20234, USA

This paper presents the results of a study of the variation of micro-indentation hardness with depth below sliding contact surfaces of OFHC Cu, Cu–3.5 wt % Al, Cu–7.0 wt % Al, and two commercial bronzes: CDA 638 and 688. All five metal alloys were worn dry against 52100 steel in a flat block (Cu alloy) on rotating cylinder (steel) configuration. The load was 10 N and sliding velocity was 20 cm sec^{-1} in a flowing argon environment. The variation of micro-indentation hardness with depth was found to be dependent upon the type of microstructural features below which each hardness profile was obtained. Therefore, micro-indentation hardness gradients sometimes varied more from location to location on a given sample than between similar microstructural features on one alloy and another. There was no obvious correlation between relative wear volumes of the alloys and the magnitude of their near surface micro-indentation hardness gradients. There did however seem to be a correlation between wear volumes and the thicknesses of highly deformed near-surface layers.

1. Introduction

Micro-indentation hardness has been used by numerous investigators to assess the extent and the characteristics of plastic deformation due to metallic wear processes (e.g. [1–6]). A common method involves cross-sectioning the worn surfaces and obtaining the "microhardness numbers"* as a function of depth below the contact surfaces. Often these cross-sections are plated to preserve their edge details during cutting and polishing because the zone of most severe deformation is often found to be very shallow (e.g. 1 to 20 μm deep). The need to use light indentation loads in sampling the microhardness numbers of these shallow zones brings with it many controversial questions which have persisted over the years without satisfactory resolution.

Attempts to do wear-hardness correlations are very common in the tribological literature. In such studies the hardness (or microhardness) of the contact surface, as opposed to the bulk hardness, is of primary interest because it reflects the properties of the zone in which wear is occurring. Because it is nearly impossible to measure the hardness by traditional indentation-based methods on a rough wear surface, attempts have been made to assign values to the surface by extrapolating data from cross-sectional hardness–depth profiles. Others, such as Richardson [5], have attempted to estimate maximum hardness by analogy with other mechanical methods producing high strains. In any event, the methodology of such studies requires careful examination.

Before the nature of near surface hardening by sliding wear-induced deformation can be adequately evaluated by the use of micro-indenta-

*"Microhardness", strictly speaking, means a very small hardness, but its conventional usage will be used in this paper to mean hardness obtained from micro-indentations.

0022–2461/84 $03.00 + .12

tions, two testing-related questions have to be addressed: (a) was sample preparation adequate to minimize artifacts in the region of interest? and (b) what intrinsic properties of the material are truly reflected in the "microhardness" numbers which are obtained?

A considerable literature exists on the subject of edge retention and damage minimization during metallographic specimen preparation. Of particular note are the fine text by Samuels [7] and the earlier books by Kehl [8] and by Goodhew [9]. Specifically with respect to sectioning of worn surfaces, Ahn *et al.* [10], Blau [11], and Torrence [12] have discussed several methods in recent publications. One difficulty in choosing the proper method for wear surface sectioning lies with the nature of the deformed zones themselves. For example, they may be preferentially attacked (due to deformation-enhanced reactivity) during attempts to use electro- or chemical-polishing, so that careful mechanical polishing often becomes the best compromise. Taper sectioning, described by Moore [13], has proven to be an effective method for enhancing the resolution of fine details near the sliding zone. Taper sectioning of electroplated surfaces of worn copper alloy samples has been used for micro-indentation studies described in this investigation.

As Moore has pointed out [13], a problem inherent in the use of the taper sectioning technique arises from the fact that an oblique plane of polish explores the microstructure at various depths below different portions of the original free surface. This should be clear from Fig. 1 (see also the Appendix). Therefore, in using the taper sectioning method in microhardness studies of wear scars it must be assumed that the hardness gradient being measured is constant along the portion of the scar immediately above the profile. Because the deep grooves on the test block scars usually extended the full length (entrance to exit end) of the scar, the assumption of gradient consistency appeared to be reasonable when profiles were taken below such long wear grooves. When microhardness profiles were obtained to compute the gradients, the samples were taper mounted such that the taper angle lay in the plane perpendicular to the original wear block surface and contained the tangential sliding direction of the ring ("transverse" taper section). The author has observed that magnitudes of microhardness gradients can vary beneath groove bottoms and beneath flat plateaus on the surface and that different modes of wear occurring in the sliding contact zone can affect such gradients [14]. Therefore only the test results for profiles taken under grooves on transverse taper sections have been compared here.

The question as to what the significance of a "microhardness number" really is will not be addressed here. This topic has been, and continues to be the subject of a vast literature. However, there seems to be a consensus of opinion that microhardness numbers arise from a combination of interactive material mechanical properties under the given testing conditions (i.e. temperature, geometry, load, etc.). There is a tendency to treat such numbers statistically, lacking a complete fundamental knowledge of their physical origins.

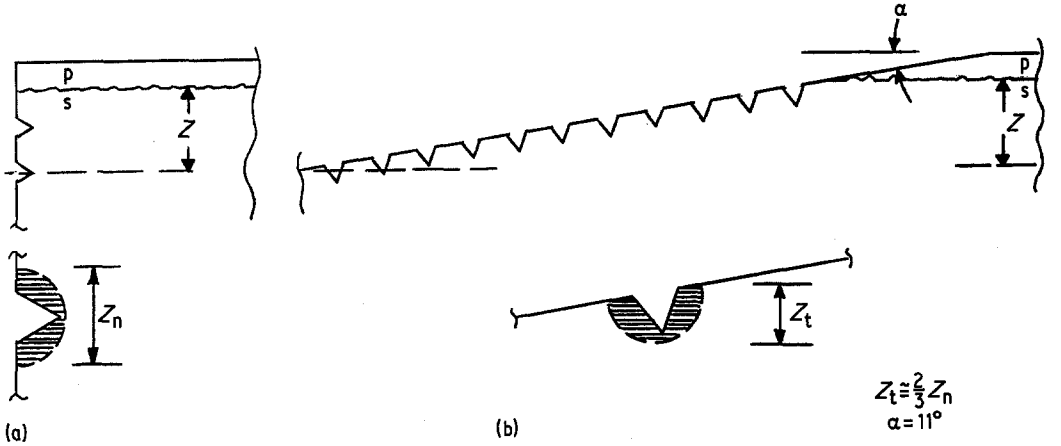

Figure 1 Illustration of the features of a normal cross-section (a) compared with a taper section (b) for micro-indentation testing. α = taper angle, p = protective plating, Z = depth to be sampled, Z_t = depth of material affected by indentaion on the taper section, Z_n = depth of material affected on the normal section, S = specimen.

the light indentation load data obtained and reported here has therefore been viewed as a relative measure of subsurface deformation rather than viewing it as a measure of a single intrinsic material property.

With the foregoing considerations in mind, the current investigation compares the nature of microhardness gradients below similar features (i.e. wear grooves) on the unlubricated sliding surfaces of copper and four copper alloys. This comparison may serve as a basis for analysing the subsurface response of several alloys to the friction forces associated with sliding wear processes.

2. Wear test method

Worn specimens were produced by sliding polished flat blocks of the five test materials against the circumferential surfaces of rotating rings of 52100 steel in the manner described by Ruff and Blau [15] and shown in Fig. 2. For each test, the applied dead weight load was 10 N, the ring's tangential sliding velocity was 20 cm sec^{-1}, and the initial surface finish of the ring surface was 0.1 to 0.2 μm (4 to 8 μ inch) rms. Flowing argon gas was used in a plexiglas enclosure to control environmental conditions (25 ± 1° C, 25 to 35% r.h.). Both ring and block specimens were cleaned ultrasonically with hexanes and acetone before mounting in the test fixture. Block specimens were mechanically polished to a final 1.0 μm diamond lapped finish the day before testing to allow a stable oxide film to form. Logarithmic oxide growth occurs rapidly in the first few minutes after polishing copper alloys [16]. Therefore, the time between polishing and testing is less critical for sequential tests on different parts of the same sample surface if the oxide growth rate is allowed to slow down and stabilize overnight. Furthermore, the final depths of the wear scars on the blocks after the standard, 1 h test lengths far exceeded any metallographically observable microstructural polishing damage on unworn portions of the test block surfaces.

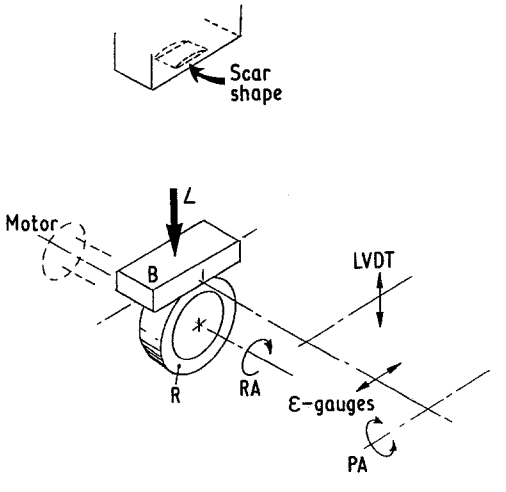

Figure 2 Geometry of the sliding wear tester. L = load, R = ring, RA = ring axis, PA = pivot axis of the block holder lever arm.

3. Metallographic specimen preparation

Taper sectioning was used to improve the spatial resolution of the microhardness against depth profiles on wear blocks. After a brief ultrasonic immersion in acetone and ethanol to remove loose debris, wear surfaces were electroplated with copper to produce a protective layer about 50 μm thick. They were then mounted in a room temperature, air-curing epoxy resin and polished by mechanical methods such that the wear scar was oriented at about 11° to the plane of polish (Fig. 1). This angle provided an apparent 5:1 magnification of surface and subsurface structures.

Using taper sections also helped to reduce the near-surface microhardness testing problems which occur when orthogonal cross-sections are used, because in taper polishing the indentation load is applied in a direction more towards the bulk material than parallel to the surface. Fig. 1 indicates this advantage schematically (also see the Appendix).

4. Microhardness test method

All testing was performed using a Knoop diamond indenter. Two different microhardness scales were used to evaluate and report test results: the standard Knoop microhardness number (KHN), and a projected area hardness (PAH). The Knoop microhardness number was calculated from

$$\mathrm{KHN} = 14\,229\left(\frac{P}{D^2}\right) \quad (\mathrm{kg\,mm^{-2}}) \qquad (1)$$

where P is the test load (g), and D is the length of the major indentation diagonal (μm). This is the equation used in the ASTM Standard Test Method E-384 [17]. It makes the assumption that the major diagonal to minor diagonal ratio of the recovered indentations remains at 7.114:1. The projected area hardness was calculated from

TABLE I Materials used in this study

Material	Nominal composition (wt%)	Grain intercept (μm) twins included	Heat treatments
OFHC Cu	99.92+% Cu	28.	Anneal at 335° C, 2 h
Cu–3.5 Al	3.5% Al, balance Cu	16.3	Cast slab ingot; final roll 50%; anneal at 535° C, 4 h
Cu–7.0 Al	7.0% Al, balance Cu	15.0	Same treatment as Cu–3.5 Al
CDA 638	3.0% Al, 1.8% Si, 0.25–0.55% Co, 0.1% Ni, 0.05% Fe, 0.5% Zn, Balance Cu	3.5	Cast; hot-rolled; anneal at 550° C, 16 h
CDA 688	3.4% Al, 0.4% Co, 22.7% Zn, 0.05 Max Pb 0.05% max Fe, 0.10% max other, balance Cu	9.4	Same treatment as CDA 638

$$\text{PAH} = 2000\left(\frac{P}{Dd}\right) \quad (\text{kg mm}^{-2}) \qquad (2)$$

where d is the length of the minor impression diagonal (μm). No presumption that the actual indenter shape is reproduced in the test piece is made in using Equation 2, only that a symmetrical diamond shape is produced. The PAH method is discussed further elsewhere [18].

5. Materials

The compositions and treatments given the test block materials are listed in Table I. The two Cu–Al binary alloys were laboratory melts; the OFHC copper and the other two multicomponent alloys were commercial materials. Heat treatments were designed to provide equiaxed grains of approximately the same size in the unworn blocks. The 52100 steel rings had a nominal composition of 1.0 wt% C–1.45 wt% Cr–0.23 wt% Si–0.35 wt% Mn–0.025 wt% mix S, P. They were obtained from a wear testing equipment manufacturer and used in the as-received condition. Their microhardness averaged KHN = 824 kg mm^{-2} (PAH = 788 kg mm^{-2}) with a 100 g load.

6. Deformed layer measurements

As previously observed by many investigators (e.g. [2, 3, 7, 10, 19]) the microstructures of many metals and alloys subjected to sliding wear contain a highly deformed layer (HDL) and a less severely deformed layer beneath it. For the purposes of this study, the latter layer will be designated the continuously strained layer (CSL) because features such as bent over grain boundaries are observed to be deformed but to remain continuous with the undistorted material in the bulk. These layers can be observed by a carefully controlled chemical etching of the taper sections. In presenting the results, estimates of the HDL thicknesses have also

TABLE II Summary of microhardness/depth data for worn specimens

Quantity	Units	Metal or alloy				
		Cu	638	688	Cu–3.5 Al	Cu–7 Al
t, HDL	μm	3.9	8.0	5.0	3.6	(9.0)*
t, CSL	μm	22.3	36.9	31.0	35.0	7.5
PAH, max	kg mm^{-2}	131	228	222	189	237
PAH_0, bulk	kg mm^{-2}	49.0	133	160	90.4	157
Linear case:						
$\text{PAH} = m_1 Z + b$						
m_1		−3.03	−1.98	−2.00	−2.15	−3.51
b		131	228	229	171	248
Corr. coef.		0.778	0.819	0.896	0.871	0.819
Exponential case:						
$\text{PAH} = \text{PAH}_0 + C_1 \exp[-C_2(Z-t)]$						
C_1		72.9	85.3	85.3	79.7	92.2
C_2		0.080	0.066	0.096	0.096	0.150
Wear vol. (two test ave.) mm^3		0.13	0.23	0.09	0.16	0.66

*May be a twinned HDL (see text discussion).

been made at the locations of the microhardness profiles. The HDL thickness was measured using either photomicrographs or the filar ocular on the microhardness tester. The thickness direction was taken to be perpendicular to the nominal horizontal wear surface (as opposed to say, the direction perpendicular to the free surface on the side of a deep wear groove).

7. Results

Microhardness profiles were obtained below wear grooves on transverse taper sections of wear blocks of the materials listed in Table I. At least two widely separated grooves were sampled on each taper section. Because the ratio of the long diagonal of the Knoop impression to the short diagonal was not generally equal to 7.114 (as implied when using the conventional KHN equation), the microhardness values were calculated by the PAH expression which uses both long and short diagonal measurements [18].

Table II summarizes the behaviour of microhardness with depth for the five metals and alloys investigated here. Two empirical fits to the data

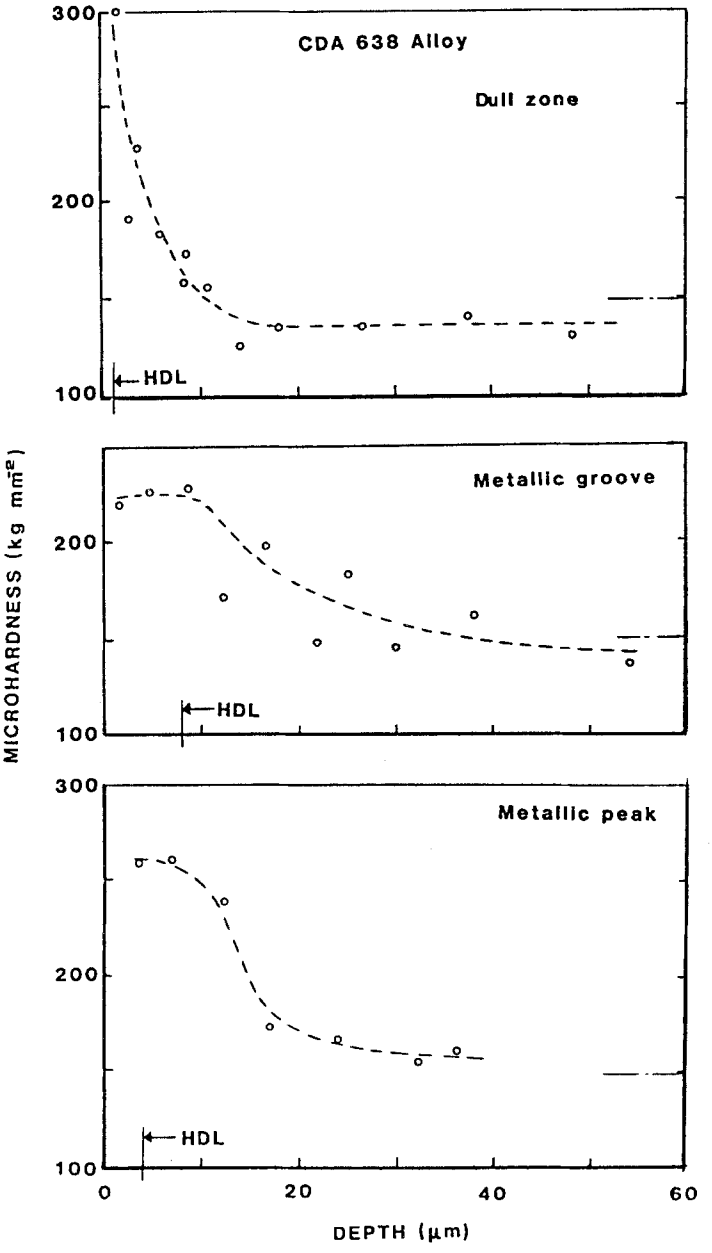

Figure 3 A plot of microhardness numbers against depth below three areas on the same wear scar.

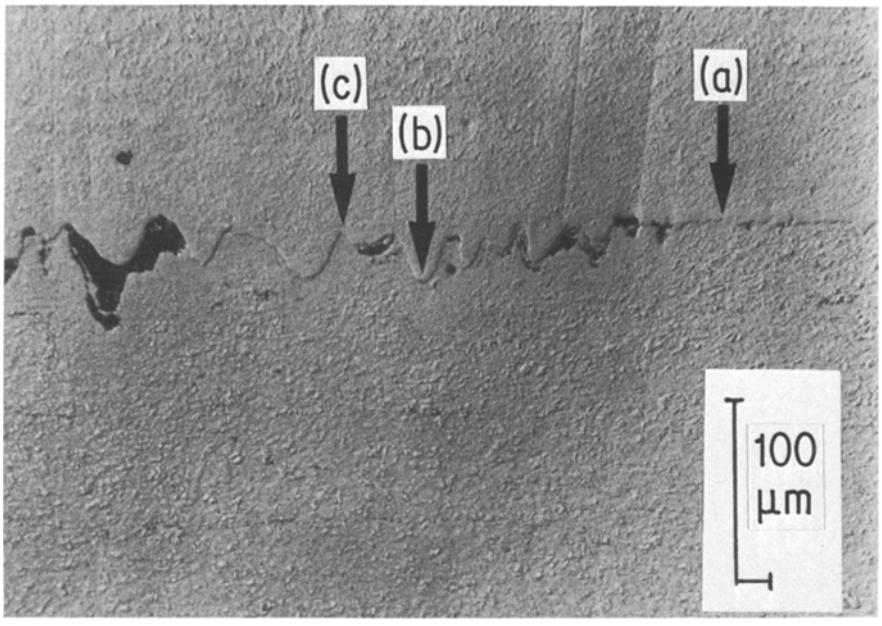

Figure 4 Microstructure of taper section of the alloy 638 worn surface showing wear grooves and the locations where the data of Table III and Fig. 3 were obtained. (a) "dull zone," (b) "groove," (c) "peak". Some dark transferred material fills the groove at the left.

were attempted: (1) a linear gradient given by

$$\text{PAH} = m_1 z + b \quad (3)$$

where m_1 and b are constants and z is depth normal to the wear surface at the location of the groove bottom, and (2) an exponential relationship given by

$$\text{PAH} = \text{PAH}_0 + C_1 \exp[-C_2(z - t)] \quad (4)$$

where, PAH_0 is the average bulk microhardness, t the HDL thickness, and C_1, C_2 are constants. Here, C_1 relates to the maximum microhardness in the highly deformed layer (or at the surface if the HDL is extremely thin). Evidence that the PAH may sometimes reach a "saturation" value below the surface can be seen in Fig. 3. The HDL was too thin to test properly even in several of the taper sections.

Wear behaviour of the five materials is also summarized in Table II. The only parameter which appears to correlate somewhat with the average block wear volume rankings is the thickness of the highly deformed layer (HDL). Such correlations have been reported previously [19]. Bulk and near-surface microhardness values do not correlate in any straightforward way with wear rankings, nor do the microhardness gradient parameters (m_1, C_1, or C_2), although the Cu–7 wt % Al had both the largest m_1 and C_1 values and the largest amounts of wear. Note that the two materials with the extremes in wear volume (i.e. the 688 alloy and the Cu–7 wt % Al) had very similar bulk and near-surface microhardnesses.

8. Discussion

As the foregoing results have indicated, it was important to compare the microhardness gradients below similar appearing microstructural features on all the alloys. That is, it would not be very reasonable to compare a microhardness profile below a flat, debris-covered plateau on one alloy wear scar with a profile below a deep wear groove on another alloy wear scar. First, we shall consider the alloy-to-alloy differences, then the possible causes for the variations between neighbouring profiles below the same scar. As noted previously, alloy-to-alloy comparisons were made for groove bottom profiles only.

The fact that the two largest linear microhardness gradients occurred on copper which wore least and on Cu–7.0 wt % Al which wore the most, leads one to the conclusion that there is no simple correlation between total sliding wear volume and the microhardness gradients below the grooves on the corresponding wear scars. It may well be that these gradients relate more to the local surface contact conditions than to the wear mechanism

TABLE III Microhardness gradients at three locations on a CDA 638 wear scar

Quantity	"Metallic" wear zone		"Dull-coloured" zone flat zone
	Groove bottom	Peak area	
Fig. 4 reference	center	bottom	top
Depth of HDL (μm)	8.0	4.0	0.9
Max. KHN near the surface ($kg\,mm^{-2}$)*	306	330	349
Max. PAH near the surface ($kg\,mm^{-2}$)*	228	261	300
Ave. bulk KHN ($kg\,mm^{-2}$)*	159 ± 4	159 ± 4	159 ± 4
Ave. bulk PAH ($kg\,mm^{-2}$)*	133 ± 6	133 ± 6	133 ± 6
Linear gradient (PAH) slope ($kg\,mm^{-2}$)*/μm	−1.98	−2.65	−12.64
Correl. coeff. for linear squares fit	0.819	0.891	0.923

*Indents at 10 g (0.098 N) load used to obtain gradients.

differences from one alloy to another; these wear mechanisms being more closely related to the properties of the highly deformed layers which lay at the uppermost bounds of the measured gradients. Therefore, in substantiation, the variation of gradients within one sample were more closely examined.

As indicated by the data from Table III and Fig. 3, a large variation was possible in the nature of the behaviour of microhardness with depth even beneath the same wear scar. This is likely to have resulted from the presence of several competing modes of wear occurring simultaneously. For example, increased clearance at one portion of the wear scar may have allowed more debris to accummulate there and act as an abrasive constituent, but conversely, debris compacts could also distribute the load more uniformly over an area and reduce the localization of stress concentrations by burying sharp asperities in a "cushion" of debris. Both the abrasivity and distribution of debris in the contact could therefore have affected the nature of the stresses acting at various locations on the wear scar: hence, the microhardness gradients may also have varied from one place to another. On scars where one mode of wear (e.g. "mild" wear with fine grooving) covers the entire contact surface one would of course expect a less drastic variation of microhardness behaviour from point to point. The subject of competition between wear modes is discussed elsewhere in greater detail [14].

The high value of microhardness on the top profile in Fig. 3 could be due to the choice of the zero reference level for the depth scales. The wear of the dull-coloured zone was less than that for the metallic zone [14]. Therefore, the sample free surface/electroplating interface which served as the zero depth reference point above each profile was closest to the level of the unworn block surface for the dull zone profile. Initially, before much wear had occurred, the scar size was smaller. Hence, the nominal contact pressure was higher. Also, debris compaction would have been in a less advanced state, and local contact stresses may have been greater at the given location leading to a greater hardening. On the other hand, if the near surface microhardness plateaus on the two lower profiles reflect the "saturation" values of microhardness, then it must be concluded that the single 300 $kg\,mm^{-2}$ value on the upper plot on Fig. 3 was spurious due to measurement difficulties for very near surface locations. This latter agrument for ignoring the high datum point would tend to level the profile plot to appear more like the lower two on the figure although the depth to reach bulk microhardness values would still be less and the magnitude of the gradient would still be higher for the topmost profile.

To illustrate one possible means to generate a truncated near-surface hardness profile, a hypothetical plot of shear stress (τ) against shear strain (γ) for a ductile polycrystalline metal has been given in Fig. 5. The yield stress (τ_y) is indicated.

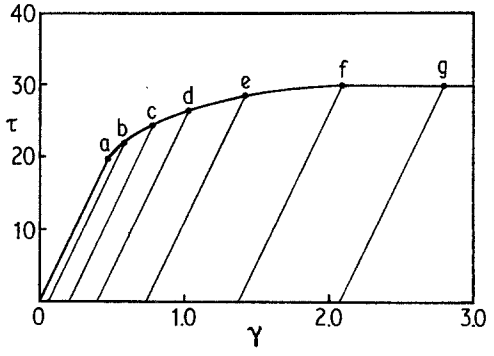

Figure 5 Typical shear stress/shear strain curve for a ductile metal. High strains are typically associated with sliding surface deformation.

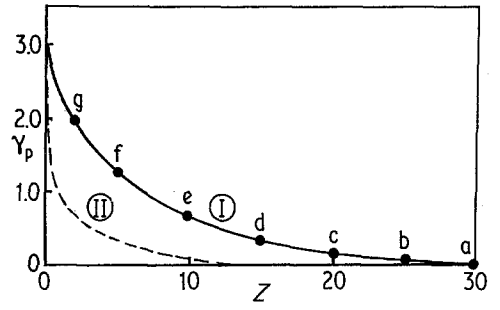

Figure 6 Two different assumed plastic shear strain gradients below a wear surface. Z = depth (typically in μm).

Note that above a shear strain of about 2.0, the stress level is nearly constant. If representative shear strain distributions below the sliding surface in the same material are given by Fig. 6 (cases I and II), one might use Fig. 5 to construct shear stress distributions for these cases. (Several investigators have experimentally obtained such microhardness and strain distributions [20–23]). After repetitive sliding events under given contact stress conditions, a residual strain distribution (e.g. Fig. 6, case I) is obtained. For each value of residual strain, one can associate a work-hardened yield stress in shear (see points a to g on the γ axis of Fig. 6). The elastic portions of the load curves have been assumed to be parallel and linear in this treatment. In this way, Fig. 7 was plotted. Note that for the two different strain gradients, there are two different reasonably linear stress gradients,

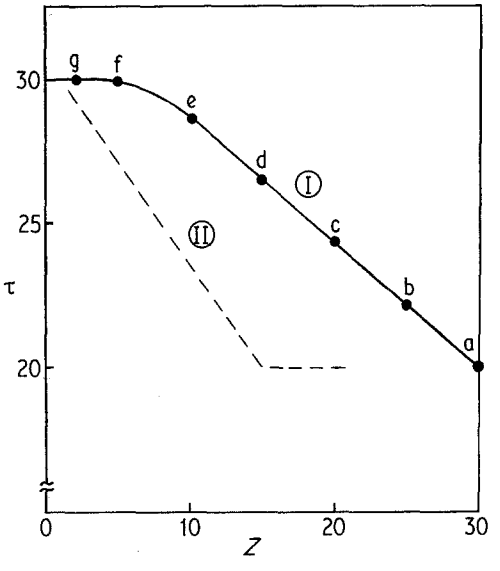

Figure 7 Shear stress distribution constructed for Fig. 5 cases using Fig. 4.

one having a plateau at the top (i.e. case I). Therefore, depending upon the contact conditions which could promote different subsurface strain distributions in the same material, one might or might not be able to detect a near surface microhardness "plateau" (assuming there that the microhardness number would behave with a fixed proportionality to shear stress). Until methods with finer spatial resolution can be found, the taper section may still be the best available technique for such studies.

Returning to Fig. 7 one observes that the truncated profile of the plots of shear strength against depth appears to correctly describe the microhardness profiles previously presented in Fig. 3. It is felt that for the homogeneous deformation of single-phase metals in sliding contact, the model proposed is a reasonable one. Unlike the model proposed for steels by Vingsbo and Hogmark [3] which involves eight metallurgical contributions (e.g. dislocation mobility, strain hardening, recovery/recrystallization, and various phase transformations), the current argument for single-phase materials is based primarily upon the assumed strain distribution and on the stress–strain relationship in a plastic material. No more detailed mechanism(s) has been considered here. The fact that the levels of the two saturation hardness plateaus in Fig. 3 were not the same may have been due to the severity of the contact conditions above the profile locations. If, during the sliding process, frictional heating was greater at one point on the surface than another, the reduction of the maximum shear stress from these localized thermal effects could have reduced the observed microhardness maxima.

To this point in the discussion, arguments for explaining the observed variation of microhardness with subsurface depth in many sliding wear studies have been based on shear strength changes due to work hardening; however, there are at least four other factors which could significantly contribute to the observed gradients (or lack thereof). These factors are:

1. crystallographic texturing due to sliding;
2. the preferred mode of near-surface deformation due to sliding;
3. the presence of localized residual stresses and how these affect hardness impression shapes; and
4. non-uniformity of the microhardness of the bulk microstructures.

Crystallographic orientation changes due to

sliding contact of metals have been recognized for a considerable time (e.g. [24–26]). In fact, at least two recent friction theories have incorporated the concept that sliding produces a reorientation (crystallographic texturing) of the near surface microstructures [26, 27]. Owing to the inherent orientation dependence of the shape and length of elongated Knoop indentations with respect to crystallographic features [28–30], it is not at all difficult to envisage how microhardness number profiles below worn, textured surfaces could be influenced by such effects. The present author has previously observed and discussed such effects as occurring in copper [6].

The mechanisms of near-surface sliding-induced deformation depend upon such material characteristics as the crystal structure(s), stacking fault energy, twin energy, and the formation of deformation-induced solid state phase changes. All these metallurgical factors and more may interact in a complex way to give rise to the metallographically observable features referred to here as the highly deformed layer (HDL) and the less deformed layer of flowed material below it (CSL). A micro-indentation placed in a region of fine twins may respond differently than one placed in a region composed of a cellular dislocation structure. Even though similar appearing HDLs can be observed (say, by lightly etching polished cross-sections) in many worn materials, their fine structures could be quite different. Investigations such as those of Ives [31], Vingsbo and Hogmark [3], and Ohmae [32] have used electron microscopy to study such fine structural details. In the case of the Cu–7 wt % Al alloy with its relatively low stacking fault energy, the deformed layers may have formed by a different mode of deformation than the other single-phase alloys and given rise to a different apparent microhardness gradient. Ramalingam and Thomann [33] have observed a transition from dislocation cell formation to twinning in single-phase (fcc) Cu–Zn alloys below a stacking fault energy of about $18\,mJ\,m^{-2}$ ($18\,ergs\,cm^{-2}$). This value corresponds to a composition between 3.5 and 7.0 wt % Al in the current binary alloy series. It is perhaps for this reason that the metallographically observed deformed layer thickness increases for the 7.0 wt % Al binary alloy after reaching a minimum at about 3.5 wt % Al. For the more complex commercial alloys with their several elemental constituents such arguments cannot be as confidently applied; however, it is reasonable to conclude that the preferred mode(s) of deformation undergone by sliding metals should have an effect on their microhardness gradients under similar test conditions.

Non-uniformly plastically deformed metals tend to have residual stresses which occur in or near the differentially deformed regions. Experiments with Knoop micro-indentations on cross-sections of bent metal sheets of copper and aluminium have demonstrated a tendency for residual stresses to affect indentation shapes depending on whether tensile or compressive stresses were applied [34]. Others have used X-ray topography to assess residual stresses near indentations [35]. Wear surfaces may also have sliding induced residual stresses. Therefore, there could also be an effect of such near-surface residual stresses on the anisotropic elastic shape recovery of micro-indentations produced at light loads on near surface cross-sections.

Recent work by Wey [36] has indicated that there was a correlation between dislocation cell size and PAH in both tension and compression tests of copper. If this relationship holds true for single-phase copper alloys as well, then samples with level microhardness plateaus near the surface should also have constant dislocation cell sizes in these regions. At the depth where the PAH begins to drop, one might expect to see either the cells increasing in size or a change in the substructural configuration (e.g. to a recrystallized zone where the cell wall stability was less and permitted grain growth to occur). Both increasing cell size and subsurface recrystallization zones were observed in the cited work by Ives [31]. Heilmann and Rigney [38] used a similar stress/strain approach in their friction model.

For polyphase, inhomogeneous alloys, however, the current model may not generally apply. For example, in sliding tests of a Cu–12 wt % Al alloy which was heat treated to produce a two-phase eutectoid structure, the microhardness variations due to indenter diagonal orientation with respect to the eutectoid microstructural constitutents were large enough to obscure the detection of any sliding-induced microhardness gradients [37]. Furthermore, the presence of the two different crystallographic phases near the sliding contact may have provided enough localized interfacial strain accommodation capacity to prevent the generation of a deeper, more extended micro-

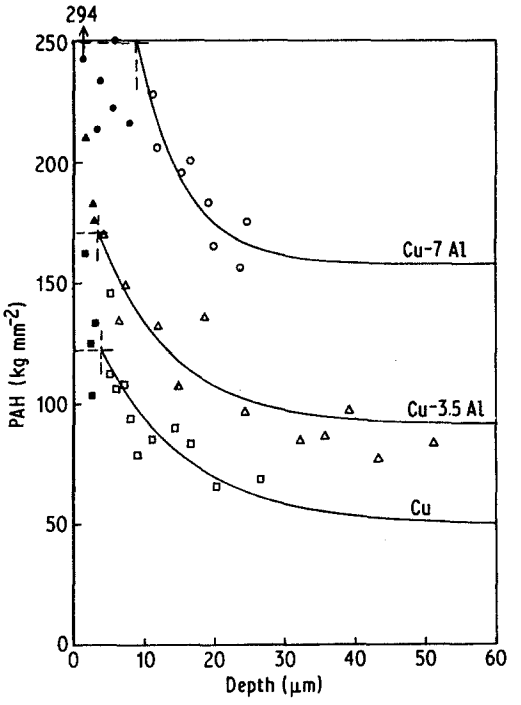

Figure 8 Plot of PAH against depth using Equation 4 for Cu, Cu–3.5 wt% Al, and Cu–7.0 wt% Al. Plots begin below the HDL depth.

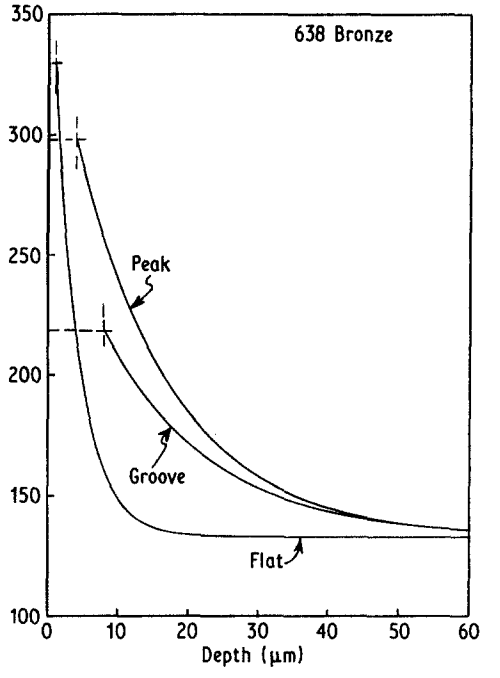

Figure 9 Plot of PAH against depth for alloy 638. Compare Equation 4 with data for three profiles shown in Fig. 3. Plots begin below the HDL depth.

hardness gradient below the surface. Therefore, the evolution of near-surface microhardness gradients during sliding also seems to be influenced strongly by both the heat treatment and by the material composition (i.e. microstructural condition).

Finally, one can examine the nature of the empirical fits for the exponential relationship of Equation 4 to the data. Plots in Figs 8 and 9 show that in general the exponential relationship worked reasonably well below the HDL. Obviously, further studies could supply the data to improve the confidence in C_1 and C_2 values. Work continues in seeking the physical interpretation of constants C_1 and C_2 from both contact conditions and from basic material properties. Hopefully, both HDL thicknesses and the subsurface microhadrness distributions from sliding wear within a host of similar materials will as a result become predictable with improved accuracy.

9. Conclusion

Variations in microhardness with depth below worn surfaces were measured on copper and four Cu–Al alloys. These gradients were measured below similarly appearing features (i.e. wear grooves) on tapered metallographic sections. On the CDA 638 alloy a large difference in the gradients due to sliding contact conditions was observed. There appeared to be no direct correlation between the final sliding wear volumes of the sectioned samples and any of the following parameters:

1. maximum near surface microhardness numbers;
2. bulk microhardness numbers;
3. local microhardness gradient magnitude (i.e. slope).

In some samples, the microhardness appeared to increase towards the sliding surface up to a maximum value then level out. This was interpreted to result from the acquisition of a maximum work-hardened shear stress state in the near-surface, highly deformed layer (HDL); however, the shear strain in this layer may have continued to increase towards the surface. The correspondence of this near surface plateau with the optically observed HDL in several samples (but not in all samples) may be due to one or more of the following factors:

1. the given HDLs were too thin to obtain an accurate plot of microhardness against depth within them (technique-limited);
2. the intrinsic HDL structure and properties in

a given material were such that its apparent thicknesse was not representative of a region of maximum shear stress, but rather represented a microstructural region whose etching response involved chemical reactivity factors not related to mechanical properties in a direct way (a material property effect);

3. microhardness numbers are not related only to shear stress; but may also relate to other parameters which vary with depth in the HDL (e.g. indenter orientation with respect to crystallographic texture).

Finally, empirical fits to plots of microhardness against depth in all five metal alloys could be produced with reasonable correlation using either linear or exponential equations, but the exponential equations seemed to lend themselves better to the physical interpretations of empirical constants.

Acknowledgements

The author wishes to thank L. K. Ives and R. deWit of the National Bureau of Standards (NBS) for their comments and discussions of the data, E. P. Whitenton of NBS for plotting and data reduction, and the Office of Naval Research for funding the wear research by which the worn samples were produced. The Cu–Al alloys were originally supplied by F. Mandigo, Olin Metals Corporation.

Appendix. Advantages and disadvantages of taper sections in microhardness profiling

Fig. 1 represents a taper section of angle α to a surface(s). The protective surface plating (p) is also indicated. The Z direction is normal to the original surface, and Z_N and Z_T represent, respectively, the volume of material affected by a micro-indentation on a cross-section perpendicular to the surface(s) ($\alpha = 90^\circ$) and by a similar micro-indentation on a taper section at some angle α to the surface. For a subsurface layer of thickness Z, many more indentations can be made on the taper section to profile the layer compared to a 90° cross-section. Also, as shown in Fig. 1, the depth of material (Z-direction) affected by each indentation on the taper section is less than that on the cross-section. Finally, the influence of the free surface and plating (p) on the very near surface indentations is reduced. The major disadvantage of the taper technique is that the location parallel to the original surface also varies laterally with depth.

References

1. J. A. KIRK and T. D. SWANSON, *Wear* **35** (1975) 63.
2. S. L. RICE, H. NOWOTNY and S. F. WAYNE, Characteristics of Metallic Subsurface Zones in Sliding and Impact Wear, Proceedings of the Conference on Wear of Materials (ASME, San Francisco, California, 1981) pp. 47–52.
3. O. VINGSBO and S. HOGMARK, Wear of Steels in "Fundamentals of Friction and Wear of Materials, (American Society of Metals, Metals Park, Ohio, 1981) pp. 373–408.
4. W. HIRST and J. K. LANCASTER, *Proc. Roy. Soc.* **A259** (1961) 228.
5. R. C. D. RICHARDSON, *Wear* **10** (1967) 353.
6. P. J. BLAU, *Scripta Metall.* **14** (1980) 719.
7. L. E. SAMUELS, "Metallographic Polishing by Mechanical Methods", 3rd Edn. (American Society for Metals, Metals Park, Ohio, 1982).
8. G. L. KEHL, "The Principles of Metallographic Laboratory Practice", 3rd Edn. (McGraw-Hill, New York, 1949).
9. P. J. GOODHEW, "Specimen Preparation in Materials Science" (North Holland/American Elsevier, New York, 1972).
10. T. M. AHN, P. J. BLAU, K-L. HSU, D. A. RIGNEY and J. J. SCHELL, *Wear* **56** (1979) 409.
11. P. J. BLAU, *Microstructural Science* **8** (1980) 369.
12. A. A. TORRENCE, *Wear* **50** (1978) 169.
13. A. J. W. MOORE, *Metallurgica* **38** (1948) 1.
14. P. J. BLAU, Competition between wear processes during the dry sliding of two copper alloys on 52100 steel, Proceedings, Wear of Materials 1983 Conference Reston, Virginia (ASME, New York, 1983) pp. 526–533.
15. A. W. RUFF and P. J. BLAU, Microscopic Aspects of Wear Processes in Metals, National Bureau of Standards, NBSIR-80-2058 (1980).
16. U. R. EVANS, "An Introduction to Metallic Corrosion" (Edward Arnold, London, 1960) p. 9.
17. American Society for Testing and Materials, Annual Book of Standards, Part II (1980) pp. 430–450.
18. P. J. BLAU, *Scripta Metall.* **14** (1980) 719.
19. P. J. BLAU, *Met. Mater. Eng.* **92** (1980) 56.
20. J. A. B. VAN DIJCK, *Wear* **42** (1977) 109.
21. D. M. TURLEY and L. E. SAMUELS, *J. Au. Inst. Metals* **17** (1972) 114.
22. J. H. DANTZENBERG and J. H. ZAAT, *Wear* **23** (1973) 9.
23. M. A. MOORE and R. M. DOUTHWIATE, *Met. Trans.* **7A** (1976) 1833.
24. H. KRAUSE and A. H. DEMIRCI, *Wear* **37** (1976) 53.
25. D. R. WHEELER and D. H. BUCKLEY, *ibid.* **33** (1975) 65.
26. D. A. RIGNEY and J. P. HIRTH, *ibid.* **53** (1979) 345.
27. D. KUHLMANN-WILSDORF, *Z. Metallkde* **72** (1981) 832.
28. E. R. PETTY, *J. Inst. Metals* **91** (1962–63) 54.
29. P. G. PARTRIDGE and E. ROBERTS, *J. Inst. Metals* **92** (1963–64), 50.

30. ASM, "The Science of Hardness Testing and Its Research Applications", Section III (American Society of Metals, Metals Park, Ohio, 1973).
31. L. K. IVES, Microstructural changes in copper due to abrasive, dry and lubricated wear, Proceedings, Wear of Materials (1979) Dearborn, Michigan, pp. 246–56.
32. N. OHMAE, Transmission electron microscope study study of the interrelationship between friction and deformation of copper single crystals, in "Fundamentals of Tribology", edited by N. P. Suh and N. Saka (MIT, Cambridge, MA 1980), pp. 201–22.
33. S. RAMALINGAM and B. THOMANN, Electron microscopy studies of chip formation in Cu–Zn alloys, Proceedings, 3rd International Conference of Precision Engineers, Tokyo, Japan (Japanese Society for Precision Engineering, Tokyo, 1977) pp. 272–277.
34. P. J. BLAU, Experiments on Knoop impression shape recovery in bent metal coupons, National Bureau of Standards (1981), unpublished research.
35. K. C. YOO, B. ROESSLER, R. W. ARMSTRONG and M. KURIYAMA, *Scripta Metall.* **15** (1981) 1.
36. Y. G. WEY, MS thesis, University of Cincinnati (1981).
37. P. J. BLAU, *Wear* **94** (1984) 1.
38. P. HEILMANN and D. S. RIGNEY, "The Running-in Process in Tribology", edited by D. Ronson, C. M. Taylor, M. Godet and D. Berthe (Butterworths, London, 1981) pp. 25–32.

Received 5 September
and accepted 22 September 1983